LANGMUIR Article
Cite This: Langmuir 2019, 35, 7322−7331
pubs.acs.org/Langmuir

Effect of Nanoscale Surface Textures on Multiphase Flow Dynamics in Capillaries

B. Liang,[†] I. M. Zarikos,[‡] W. B. Bartels,[‡] S. M. Hassanizadeh,[‡] and A. Clarens*[,†]

[†]Engineering Systems and Environment, University of Virginia, 351 McCormick Road, Thornton Hall, Charlottesville, Virginia 22904, United States

[‡]Department of Earth Sciences, Faculty of Geosciences, Utrecht University, Utrecht 3508 TA, The Netherlands

Supporting Information

ABSTRACT: Multiphase flow through porous media is important in a wide range of environmental applications such as enhanced oil recovery and geologic storage of CO_2. Recent in situ observations of the three-phase contact line between immiscible fluid phases and solid surfaces suggest that existing models may not fully capture the effects of nanoscale surface textures, impacting flow prediction. To better characterize the role of surface roughness in these systems, spontaneous and forced imbibition experiments were carried out using glass capillaries with modified surface roughness or wettability. Dynamic contact angle and interfacial speed deviation, both resulting from stick-slip flow conditions, were measured to understand the impact these microscale dynamics would have on macroscale flow processes. A 2^k factorial experimental design was used to test the ways in which the dynamic contact angle was impacted by the solid surface properties (e.g., wettability, roughness), ionic strength in the aqueous phase, nonaqueous fluid type (water/Fluorinert and water/dodecane), and the presence/absence of a wetting film prior to the imbibition of the wetting phase. The analysis of variance of spontaneous imbibition results suggests that surface roughness and ionic strength play important roles in controlling dynamic contact angle in porous media, more than other factors tested here. The presence of a water film alone does not affect dynamic contact angle, but its interactions with surface roughness and aqueous chemistry have a statistically significant effect. Both forced imbibition and spontaneous imbibition experiments suggest that nanoscale textures can have a larger impact on flow dynamics than chemical wettability. These experimental results are used to extend the Joos and Wenzel equations relating apparent static and dynamic contact angles to roughness, presence of a water film, and water chemistry. The new empirical equation improves prediction accuracy by taking water film and aqueous chemistry into account, reducing error by up to 50%.

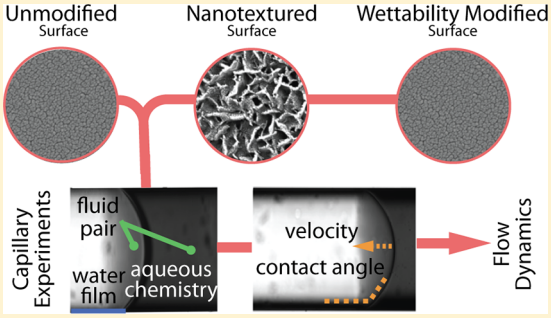

INTRODUCTION

A number of naturally occurring and engineered processes in the environment involve the flow of multiple phases through porous media.[1] Processes such as groundwater remediation, geologic carbon storage, enhanced geothermal energy production, and enhanced oil recovery are impacted by the porosity, pore geometry,[2] viscosity ratio of fluids,[3] flow conditions,[4] interfacial tension (IFT),[5] fluid dynamics[6,7] and wettability of the host rock.[4,8,9] Wettability, in particular, has been widely known to impact these flow processes,[10] but recent work using new in situ imaging techniques suggests that small-scale (e.g., nanoscale) roughness or texturing on the mineral surface strongly impacts wettability,[11,12] which can, in turn, impact fluid flow processes.[13,14] These findings are consistent with much of the recent work focused on designing superhydrophobic or superhydrophilic surfaces, which rely in large part on the nanoscale structure at the surface.[15,16] The impact that these types of features would have on flow in a complex heterogeneous rock formation has not been studied to date.

The role of roughness on interfacial forces acting on an apparent static three-phase contact line (Figure 1) has been considered extensively in the literature starting with the work of Wenzel and Cassie−Baxter.[17,18] Wenzel's model predicts that the wetting phase will completely penetrate the surface asperities on a rough surface and that for a hydrophilic solid surface, this process will enhance wetting. Cassie modeled interfacial energy as a function of the structure of the solid surface, suggesting that the nonwetting phase fluid can get trapped in the pockets on the surface. Like most models of wettability, these are based on the relationship between fluid flow dynamics and the fluid−solid interaction. The difference between the Wenzel and Cassie−Baxter models, related to the presence/absence of a continuous wetting film, is depicted in Figure 1.

The presence or absence of a wetting film has been shown to play an important role in multiphase flow on rough surfaces.[19] During imbibition of the wetting phase, a thin film of wetting phase can make the effective surface roughness of solid much

Received: January 2, 2019
Revised: April 29, 2019
Published: April 29, 2019

DOI: 10.1021/acs.langmuir.8b04320
Langmuir 2019, 35, 7322−7331

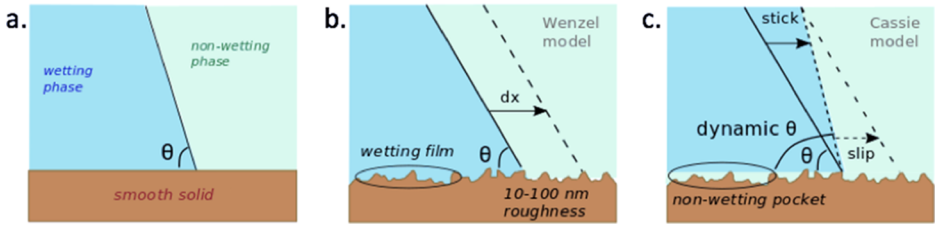

Figure 1. Illustration of multiphase flow across surfaces with a (a) smooth surface; (b) prewetted rough surface with a film of the wetting phase filling in the asperities (i.e., the Wenzel model); and (c) rough surface with nonwetting phase filled in the asperities that leads to stick-slip flow (i.e., the Cassie model).

less pronounced. The existence and swelling of the wetting film could also lead to snap-off of the nonwetting phase,[20] which is a critical part of the displacement process. In the context of groundwater remediation, for example, the thickness of the water film is proportional to the underlying solid surface roughness.[21] In CO_2 storage, water films have been shown to exist during CO_2 injection and to become thinner as pressure increases and the surface becomes more negatively charged as CO_2 dissolves into the film,[22] which enables changes in solution chemistry.[23]

Experimental observations, such as contact line pinning or adhesion, are often attributed to these microscale characteristics related to surface textures and wetting.[12,24] This roughness contributes, at least in part, to the development of stick-slip flow behavior at the interface.[25,26] In the context of environmental systems, stick-slip flow can have complex impacts on multiphase flow in porous media, especially at low Capillary numbers.[27,28] At low velocity, irregular movement of the interface in the pores can impact the stability of the system at macroscales. For example, in cases where the residual saturation of the nonwetting phase has been reached, the instability of interface between the continuous wetting phase and a nonwetting phase cluster could result in the mobilization or break up of that cluster.[29] Stick-slip flow can also impact the connectivity of fluids in a porous medium, which impacts ganglion dynamics.[30]

The wettability of two fluids on a solid surface is directly impacted by interfacial forces (e.g., interfacial tension) between those fluids.[31] Interfacial tension is an aggregated measure of the cohesive forces and adhesive forces between the fluid phases and therefore depends on the fluid chemistry.[32] In aqueous systems, ion concentration and composition play an important role in driving interfacial tension and ultimately capillary pressure. The ionic composition of water can also impact the charged functional groups on the solid surface.[33] Although much fundamental work has been carried out in recent years to catalog and describe the impact of mineral chemical heterogeneities on wettability, less work has focused on how textures in different rock types that originated via diagenetic processes might impact multiphase flow.[34]

These processes are generally described using the Washburn equation.[35] The Washburn equation is a dynamic energy balance on idealized fluid flow through a single capillary with a uniform circular cross-section under the laminar flow conditions. Although some of these conditions (e.g., uniform cross-section) are not representative of many environmental porous media, the majority of the assumptions (e.g., incompressible and Newtonian) are valid in many contexts. The model is typically written as

$$\sum P = \frac{8\mu l Q}{\pi r^4} \tag{1}$$

where $\sum P$ is the total pressure difference between two phases (the sum of the external pressure, ΔP, and capillary pressure, $P_c = \frac{2\gamma \cos\theta}{r}$, where θ is the contact angle and γ is the interfacial tension), i.e., $\sum P = \Delta P + P_c$. μ is the fluid viscosity, l is the length of the capillary, Q is the volumetric flow rate, and r is the radius of the capillary.

Substituting these two pressure expressions into the Poiseuille equation, the Washburn equation can be written as

$$\Delta P + \frac{2\gamma \cos\theta}{r} = \frac{8\mu l}{r^2}\left(\frac{\mathrm{d}l}{\mathrm{d}t}\right) \tag{2}$$

where $\frac{\mathrm{d}l}{\mathrm{d}t}$ is the interfacial velocity. The adoption of the Washburn equation has significant impacts in relating interfacial properties and capillary pressure in the fluid system. An important limitation when applying this equation is the single term of contact angle θ, which is usually measured as the apparent contact angle. In reality, fluids in motion often have a different contact angle than they do at equilibrium,[19] and so a dynamic contact angle is a more appropriate measure for fluids with a nonzero interfacial velocity. The relationship between equilibrium (θ_e) and dynamic (θ_d) contact angles over a perfectly smooth surface is known to be a function of fluid velocity

$$\theta_d = f\left(\frac{\mathrm{d}l}{\mathrm{d}t}, \theta_e\right) \tag{3}$$

Both analytical and empirical methods have been used to explore the relationship between θ_d and θ_e. Sheng[36] and Popescu[37] developed analytical hydrodynamic relationships based on viscous energy dissipation. Brochard-Wyart[38] used a molecular dynamic approach, based on the relationship between the displacement of fluid molecules and the movement of the contact line. These approaches have been used by Blake[39] to develop a hydrodynamic and molecular kinetic model. The resulting equations are generally good predictors of experimental observations in a gas−liquid system but do not capture the behavior of liquid−liquid systems particularly well. This could be because both hydrodynamic and molecular kinetic analyses are based on the assumption that one phase dominates the flow momentum, as would be the case for fluid pairs with a large viscosity ratio.

In an effort to develop empirical relationships that work for a broader range of fluid pairs, Joos[40,41] conducted capillary rise experiments and used the Washburn equation with modified dynamic contact angle to match experimental data, proposing the following correlation

$$\cos\theta_d = \cos\theta_e - \alpha(1 + \cos\theta_e)Ca^{1/2} \tag{4}$$

DOI: 10.1021/acs.langmuir.8b04320
Langmuir 2019, 35, 7322−7331

where α (found to be 2 in the original experiments by Joos et al.[41]) is a coefficient that has been reported to vary with fluid properties, and the interface velocity $\left(\frac{dl}{dt}\right)$ is incorporated into the capillary number ($Ca = (\mu v)/\gamma$, μ is the fluid viscosity, v the velocity of contact line, and γ is the interfacial tension). Cox[42] and others have expanded this correlation more recently for a wider range of geometries, capillary numbers, and fluid pairs. Despite these advances in fundamental wettability theory and more recent applied characterization under reservoir conditions,[43−45] the role that surface textures have on the flow dynamics has not been explored in a way that enables easy comparison with other factors understood to impact multiphase flow.

To build on the understanding developed by Joos and Wenzel, we carried out a set of controlled experiments in glass capillaries to test a number of hypotheses related to the impact of nanoscale surface textures on multiphase flow. The first hypothesis was that nanoscale textures will impact flow dynamics and that these effects would be stronger when coupled with other systems properties such as higher ionic strength solutions, higher flow rates, and the presence/absence of a wetting film. The second hypothesis was that these texture effects could have a greater impact on fluid flow dynamics than chemical wettability. Single-capillary glass micromodels were used to enable easy visualization and control of flow properties. Both spontaneous and forced imbibition experiments were conducted to collect data over a wide range of capillary numbers. The experimental results were then interpreted in the context of modeling frameworks to extend predictive capabilities.

EXPERIMENTAL SECTION

Micromodel Fabrication. Soda lime glass capillaries (Hilgenberg GmbH) with an external diameter of 0.82 mm and an internal diameter of 0.64 mm were modified to generate either a nanotextured surface roughness or to increase their wettability with respect to water. Alkali etching was used to generate submicron surface features on the glass surface.[31,46] Compared to other dry etching techniques and HF-based etchants, aqueous-based alkali etching is safer and simpler and capable of achieving extreme wettability (superhydrophilicity and superhydrophobicity) and associated properties such as antireflection[47] and low dielectricity.[48] The dimension and morphology of surface texture were controlled by changing the etching time, temperature, and glass chemical composition.[47,49] The glass capillaries were first cleaned in demineralized water and then with a 1:1:1 volume mixture of acetone, methanol, and trichloroethylene under sonication. The cleaned capillaries were placed in a sealed vessel containing an aqueous solution of 0.2 mol/L KOH and then heated at 95 °C for 24 h to enable chemical etching. Following etching, the capillaries were rinsed with demineralized water, then again with the acetone, methanol, and trichloroethylene solution under sonication, and finally with demineralized water. The capillaries were dried using compressed air between each treatment.

The validation and quantification of the etching were carried out using scanning electron microscopy (SEM) observations and energy dispersive X-ray spectrometry (FEI-650). The effect of the etching process on the glass surface is shown in Figure 2. The surface asperities created in this etching process were between 10 and 100 nm long. Using a Zygo Newview 7300 noncontact profilometer, we confirmed that the characteristic lengths (both depth and lateral length) of the nanostructured features are on the order of tens of nanometers, which is consistent with other studies that deployed similar etching techniques. The etching process also changed the ionic surface composition of the underlying glass itself, as ions are lost to the aqueous phase due to hydrolysis and ion exchange during the

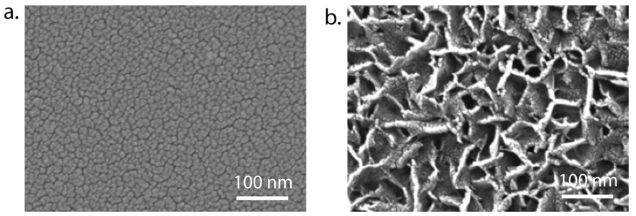

Figure 2. Surface micrographs of (a) untreated and (b) etched glass capillary.

treatment.[47] The net effect of these physical and chemical alternations was that the glass increased the hydrophilicity of the surface significantly, which was observable as the glass surfaces exhibited smaller contact angles and more pronounced capillary action, as expected based on the Wenzel theory.

To create wettability-modified samples, a separate group of capillaries was treated using oxygen plasma to make the surfaces more water wetting without changing the surface roughness. Plasma treatment works by enabling electron transfer between ions in the solution and the glass surface, neutralizing the dissolved ions and creating a more positively charged surface layer on the glass. Oxygen plasma treatment was carried out using a South Bay Plasma System (PC 2000) for 10 min. Cleaned capillaries were put into the plasma chamber and aligned with the two discharge ends. After treatment, the wetting properties of the treated capillaries were measured using contact angle and capillarity experiments. The surface structure was examined using SEM to confirm that no additional roughness had been introduced.

Experimental Setup. Imbibition experiments were carried out in capillary samples, where the nonwetting phase was displaced by the wetting phase. Both spontaneous and forced imbibition experiments were carried out to cover as wide a range of capillary numbers as possible. The capillary was initially saturated with the nonwetting phase. To ensure the absence of water film on the walls of the capillary, the capillary was oven dried at 90 °C prior to the initial saturation. After the initial saturation with the nonwetting phase, the wetting phase was imbibed. The same protocol was followed for every set of experiments.

Fluorinert FC-43 and dodecane were used as the two nonwetting fluids in the experiments. Fluorinert FC-43 is a colorless, inert fluorocarbon that is a liquid at 1 atm and 25 °C (refraction index, n = 1.291). It is 4.7 times more viscous and 1.86 times heavier than water ($\mu = 4.7 \times 10^{-3}$ Pa s, $\rho = 1860$ kg/m^3). Dodecane, on the other hand, is less viscous and lighter than water ($\mu = 1.36 \times 10^{-3}$ Pa s, $\rho = 749$ kg/m^3). Ecoline 578 ink was added to water to improve contrast under the microscope. To investigate the combined effect of roughness and different values of interfacial tension, the chemistry of the wetting phase was modified by the addition of NaCl into the solution. When the dye was mixed with deionized (DI) water, its interfacial tension with Fluorinert was 58 mN/m.[31] When NaCl was added to the water-based dye to increase its ionic strength, the interfacial tension dropped to 35 mN/m.

Spontaneous Imbibition Experiments. Capillaries were filled with the nonwetting phase and positioned vertically in a stand above a Petri dish containing the wetting phase. At the start of each experiment, the capillary was lowered into the container so that the bottom edge came in contact with the wetting phase, which rose through the capillary as a result of capillary forces. A high-speed camera (Memrecam GX-1, NAC) equipped with a microlens (AF Micro-NIKKOR 200 mm, Nikon) was used to capture images of the interface. A frame rate of 10 000 fps was used to capture images in our experiments at a resolution of 512 × 384. A pair of light-emitting diode lights (uLite 2-Light Octabox 200 W Fluorescent Kit, Westcott) was used to provide an optimal contrast between fluids. The contact angle for the images was measured using ImageJ with the Drop Analysis plugin.[50] The apparent contact angles for each combination of solids and fluid pairs were measured before the experiments, on glass microscope slides. For each

DOI: 10.1021/acs.langmuir.8b04320
Langmuir 2019, 35, 7322−7331

experiment, at least nine pairs of contact angles were measured, and data were compiled for statistical analysis.

Forced Imbibition Experiments. Capillaries were aligned horizontally in the field of view of a Nikon A1R confocal microscope. The fluid input was controlled with the use of a Harvard Picoplus syringe pump using a Hamilton 7000 series glass syringe. Two syringes containing the wetting and the nonwetting phase fluids were connected to the inlet holes of a T-section type connection. The syringe with the wetting phase was connected to the syringe pump, whereas the other was controlled manually. A valve placed between the T-section and the nonwetting phase syringe was closed during imbibition, to ensure flow in the desired direction. The capillary was placed and secured under the microscope, and finally the outflow was connected to a drain. The whole set up was installed on a vibration-free table. The field of view was monitored optically with a DS-Ri2 camera with a resolution of 16.25 megapixels (resolution 2.46 μm/pix, at 10× magnification) which can record high-resolution images at a stable frame rate of 20 fps. We used confocal laser scanning microscopy to identify the presence or absence of a water film and also investigate its thickness and structure. For this, we used an LU-N3 laser unit, set up at 488 nm, an A1-DU4, set up to 525 nm, and a high-resolution Galvano scanner, set up at 1.24 μm/pix, at 10× magnification. The movement of the liquid–liquid interface along the capillary was analyzed with the NIS Element software, part of the Nikon A1R microscope. The image tracking data were used to calculate the velocity of the center of the interface between wetting and nonwetting fluids as a function of time under constant flow conditions. The standard deviation of the velocity data was used to calculate a measure of the overall stick-slip behavior of the interface.

Experimental Design. Four independent variables were included in a modified 2^k factorial design of experiments: surface treatment (three levels: untreated, roughened, or wettability modified), presence of a water film (two levels: present or absent), aqueous chemistry (DI water or 1 M NaCl solution) and nonaqueous fluid type (Fluorinert or dodecane), as shown in Table 1. This approach allowed us to investigate the contribution of each independent variable and the interaction effects between these on the dependent variables. Setting up the experiments in this way enabled us to perform the analysis of variance (ANOVA) on the results. Replicates of each experiment were carried out, and normal distributions for the results were visually examined and quantified using a Tukey test with a quantile–quantile plot. A Tukey test is a single-step statistical test to find mean values that are significantly different from one another. Levene's method was then used to test that the variance between samples is equal, and there is no statistically significant difference in variance across experimental conditions.[27,28]

Table 1. Factorial Design of Experiments Used To Develop the Experimental Matrix Presented Here

exp. #	surface treatment	wetting film	aqueous chemistry	nonaqueous fluid
1	untreated	no	DI water	Fluorinert
2	untreated	yes	DI water	Fluorinert
3	roughened	no	DI water	Fluorinert
4	roughened	yes	DI water	Fluorinert
5	wet modified	no	DI water	Fluorinert
6	wet modified	yes	DI water	Fluorinert
7	untreated	no	1 M NaCl	Fluorinert
8	untreated	yes	1 M NaCl	Fluorinert
9	roughened	no	1 M NaCl	Fluorinert
10	roughened	yes	1 M NaCl	Fluorinert
11	wet modified	no	1 M NaCl	Fluorinert
12	wet modified	yes	1 M NaCl	Fluorinert
13	untreated	no	DI water	dodecane
14	untreated	yes	DI water	dodecane
15	roughened	no	DI water	dodecane
16	roughened	yes	DI water	dodecane
17	wet modified	no	DI water	dodecane
18	wet modified	yes	DI water	dodecane
19	untreated	no	1 M NaCl	dodecane
20	untreated	yes	1 M NaCl	dodecane
21	roughened	no	1 M NaCl	dodecane
22	roughened	yes	1 M NaCl	dodecane
23	wet modified	no	1 M NaCl	dodecane
24	wet modified	yes	1 M NaCl	dodecane

RESULTS AND DISCUSSION

Capillary imbibition experiments were performed over a range of velocities/capillary numbers to test our hypotheses related to the influence of nanoscale roughness on multiphase flow in capillaries. In both experimental setups used here, the three-phase contact line was carefully monitored to evaluate the dynamic contact angle (at higher capillary numbers) and the standard deviation of interface velocity (at lower capillary numbers). These metrics are both connected to stick-slip behavior, which are short-term (i.e., on the order of milliseconds) accelerations and decelerations. The resulting stick-slip flow would influence pore-scale flow dynamics such as snap-off during imbibition and Haines jump during drainage.[27]

Spontaneous Imbibition Experiments. To test the first hypothesis that nanoscale textures will impact flow dynamics and that these effects would be stronger when coupled with other system properties, such as higher ionic strength solutions, higher flow rates, and the presence/absence of a wetting film, the dynamic contact angle of fluid pairs was measured for all of the conditions listed in Table 1. The results are presented in Figure 3. In this figure, the experimental results are binned based on the aqueous chemistry and the surface treatment of the capillary for the two fluid pairs tested here (Figure 3a shows water and Fluoroinert and Figure 3b shows water and dodecane). The data show considerable scatter but there seems to be some order to the results across conditions. For example, the untreated surfaces with high NaCl water tended to have higher dynamic contact angles.

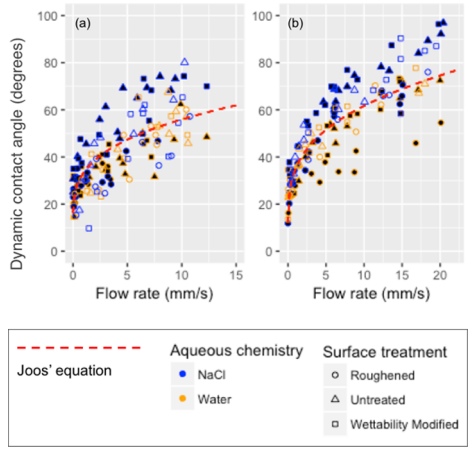

Figure 3. Dynamic contact angle of the interface between water and (a) Fluorinert and (b) dodecane, as a function of flow rate, surface treatment, aqueous chemistry, and water film. Hollow symbols indicate experiments with no water film and filled symbols represent experiments where a water film was present.

The least-square-root fit of the data was performed using the Joos equation modified using the Wenzel theory, and those are

DOI: 10.1021/acs.langmuir.8b04320
Langmuir 2019, 35, 7322–7331

Table 2. ANOVA Results for Dynamic Contact Angle Data Collected during Spontaneous Imbibition Experiments as a Function of Various Independent Variables[a]

independent variable and interactions	Df	mean sq	*F*-value	*p*-value
surface	2	6207	27.13	2.89×10^{-11}
aqueous chemistry	1	7953	34.76	1.38×10^{-8}
water film	1	223	0.98	0.32
nonaqueous fluid	1	4031	17.62	3.91×10^{-5}
surface + aqueous chemistry	2	541	2.37	0.10
surface + water film	2	1575	6.89	1.34×10^{-5}
aqueous chemistry + water film	1	1025	4.48	0.04
surface + nonaqueous fluid	2	194	0.85	0.43
aqueous chemistry + nonaqueous fluid	1	483	2.11	0.15
water film + nonaqueous fluid	1	6	0.03	0.86

[a]Df (degrees of freedom) is a measure of the independent pieces of information for a particular variable; mean sq (mean squares) is an estimate of the variability in the response data that attributed to each independent variable; the *F*-value is the ratio between factor mean squares and the residual mean squares; and the corresponding *p*-value is used to determine the statistical significance in the hypothesis test, so values that are less than the significance level, in this case 0.05 (corresponding to 95% confidence), are highlighted to show those effects with a statistically significant impact on the dynamic contact angle.

plotted in Figure 3 as dashed lines. The Wenzel model defines an apparent contact angle for rough surfaces as

$$\cos\theta^* = r\cos\theta \tag{6}$$

where θ^* is the apparent contact angle on a rough surface, θ is the Young contact angle on an ideal flat surface, and r is the roughness ratio, defined as the ratio of the true area of solid surface to the apparent area. Combining this with the Joos equation (eq 4) to account for the surface roughness yields

$$\cos(\theta_d) = r\cos(\theta_e) - \alpha(1 + r\cos(\theta_e))Ca^{1/2} \tag{7}$$

where θ_d is the dynamic contact angle and θ_e is the contact angle at equilibrium. The model results in Figure 3 were obtained by fitting the dynamic contact angle data under two flow rate conditions, in which the parameters α and r are derived by least-square fit. The best fit r value is 1.36−1.49 for the two different fluids, which is within the range of measured values. This combination of Joos' model and Wenzel's law effectively predicts the general correlation between the dynamic contact angle and flow rate, but given the other trends in the data that emerge from the various conditions tested here, it seems that an improved model may be able to quantify the relationship between flow velocity and dynamic contact angle taking into account other important parameters like ionic strength and roughness.

Impact of Surface Features, Water Film, and Solution Chemistry. To develop a more refined understanding of the factors controlling this system, the effect of independent variables and their interactions on the dynamic contact angle was analyzed by performing an ANOVA on the complete dataset for the spontaneous imbibition experiments. The results are presented in Table 2, based on the Tukey statistical test, where $p < 0.05$ is used to establish statistical significance. The *p*-value is calculated from the *F*-value, which is a function of mean squares (sum of squares (SoS) divided by degrees of freedom). It should be noted that since three surface treatments are presented, the surface variable and its interaction with other variables have a degree of freedom of 2, where the other variables have a degree of freedom of 1.

The results show that surface treatment and aqueous chemistry have a statistically significant impact on the dynamic contact angle, whereas the water film alone does not. The nonaqueous fluid (Fluorinert or dodecane) shows an effect, but no interaction with any other factor tested here. This suggests that the trends observed could be applied to other fluid systems more generally. Several two-way interactions are also important, namely, the interaction between aqueous chemistry and water film and the interaction between surface and water film. In ANOVA, two- and three-way interactions can be understood as the effect of one or two variables across the levels of another. It is interesting to note that the presence of a water film by itself does not impact the results, but it accounts for a large portion of the variance when combined with surface or aqueous chemistry. None of the interactions between any three of the independent variables had a statistically significant effect, and so those are not included in Table 2. The full ANOVA results are presented in the Supporting Information.

As the ANOVA results presented in Table 2 suggest, the most important factors influencing the dynamic contact angle individually are surface treatment, aqueous chemistry, and the nonaqueous fluid because they have *p*-values significantly lower than 0.05. The water film does not have a strong impact as a single factor, but its interaction with aqueous chemistry is a statistically significant effect. To better illustrate this interaction effect, results are plotted in Figure 4 as two separate panels with and without the water film. When no water film is present,

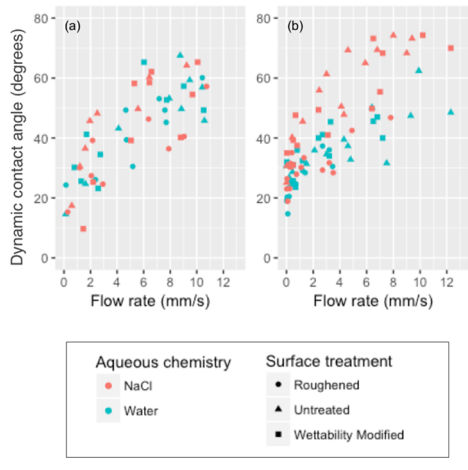

Figure 4. Dynamic contact angle for different surfaces and solution chemistry (a) with and (b) without a wetting film.

DOI: 10.1021/acs.langmuir.8b04320
Langmuir 2019, 35, 7322−7331

water and NaCl results are distributed in the same cluster, however, when a water film exists, dynamic contact angles are considerably larger when NaCl is in the solution.

The interaction effects between surface roughness, presence of a wetting film, and ionic strength in solution can be understood in terms of electrostatic interactions and disjoining/conjoining pressure at the liquid meniscus. Salinity impacts the interfacial tension (IFT) between the fluids. For the Fluorinert/water system, for example, the addition of 1 M NaCl lowers the IFT from 58 to 35 mN/m, which makes the capillary more water-wetting. This effect would be even more pronounced for more complex ionic solutions. Aggelopoulos[51] showed that divalent cations influence wettability even more strongly than the monovalent ions tested here. These ions also interact with the charged silica surface including the electrical double layer[24,52] near the surface. Higher concentrations of ions provide additional electrostatic force,[52] which can offset some of the increased contact angle due to changes in the IFT.[53,54] The presence/absence of a water film changes the acting forces at the three-phase contact line. The disjoining/conjoining pressure at the three-phase contact line also contributes to variations of surfaces forces, which include electrostatic, van der Waals, and structural components.[55] Without a water film, surface pinning contributes to stick-slip flow,[56] which we observed. Taken together, these results suggest that surface roughness and water film could play important roles in multiphase flow dynamics, particularly at higher ionic strengths, where the interplay between interfacial tension, electrokinetic interactions, and interface disjoining/conjoining pressure impacts the dynamic flow. Therefore, there is a clear need to improve the empirical equation to capture these processes.

Derivation of an Improved Modeling Framework. As shown in Figure 3, the Joos and Wenzel equations (eq 7) capture the general relationship between dynamic and static contact angles but cannot account for the large amount of scatter in the data that emerges from varying key system parameters. This result was expected given that the model only has one fitting parameter, α ($\alpha = 0.47$). To incorporate some of the qualitative findings from the ANOVA, we extend eq 7, adding an additional fitting parameter

$$\cos(\theta_d) = r\cos(\theta_e) - \alpha[(\beta + r\cos(\theta_e))]Ca^{1/2} \quad (8)$$

where β is a second fitting parameter obtained from our data. Although both α and β could be used to get the best fit for each experimental condition, we propose to treat them as empirical constants that are tied to a physical characteristic of the system. α is related to the presence of a water film, and β is related to the ionic strength of the aqueous phase

$$\cos(\theta_d) = r\cos(\theta_e) - \alpha(\mathrm{wf}) \times [(\beta(\mathrm{ac}) + r\cos(\theta_e))]Ca^{1/2} \quad (9)$$

where

$$\alpha(\text{water film[wf]}) = \begin{cases} 0.415, \text{ when wf} = 1 \\ 0.640, \text{ when wf} = 0 \end{cases}$$

and

$$\beta(\text{aqueous chemistry[ac]}) = \begin{cases} 1.21, \text{ when ac} = \text{NaCl} \\ 0.903, \text{ when ac} = \text{DI water} \end{cases}$$

Figure 5 presents the relationship between flow rate and dynamic contact angle for a representative experiment along

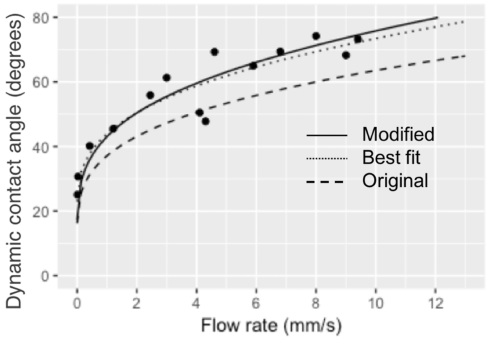

Figure 5. Comparison of models fitted on experimentally measured dynamic contact angle data for Fluorinert/NaCl solution on an untreated wet surface.

with different fitting equations. These fitting parameters (α and β) are tied to physical characteristics of the system that will provide better resolution of dynamic flow properties in multiphase systems. The two-level experimental set up used here did not enable us to fully quantify the strength of effect such that α and β could be characterized for a much wider range of conditions and their magnitude could be defined proportional to the characteristics of the water film (e.g., thickness, continuity, etc.) or the aqueous chemistry (e.g., ion composition, concentration, etc.), but subsequent work might further develop these parameters. Nevertheless, the addition of these fitting parameters does capture physical elements of these flow systems that existing modeling frameworks cannot, and that will improve the utility of these modeling approaches.

To account for the benefit associated with adding these parameters to the equation,[57] the goodness of fit is evaluated by a modified root-mean-square error (RMSE), which is defined as

$$\mathrm{RMSE} = \left(\frac{\mathrm{RSS}}{m - p}\right)^{1/2} \quad (10)$$

where RSS is the residual sum of squares, m is the number of observations, and p is the number of adjustable parameters. The modified Joos–Wenzel equation (eq 7) is shown as the dashed line. In this case, it underestimates the increase of dynamic contact angle, resulting in a RMSE of 14.6°. The best fit (eq 8) is the least square fitting for a specific condition with α and β as fitting parameters, representing the lowest possible RMSE of 4.6. The newly proposed equation (eq 9) uses the global constants α and β and compares well with the best fit (RMSE of 4.8° in this case).

Equation 9 was used to fit all spontaneous imbibition experimental data collected in this study, and representative results are presented in Figure 6. Here, we compare its fitting performance to the roughness-modified Joos equation (eq 7), on Fluorinert contact angle with a water film. In general, the average RMSE between the data and model fit is reduced from 9.8° using eq 7 to 5.7° using the newly proposed eq 9. This improvement is especially significant when ionic strength is higher, where it interacts with surface features, and therefore has co-effects that are not captured by the original model. The single set RMSEs for Figure 6b (untreated surface) and Figure 6d (roughened surface) are both reduced by more than 65% from the original model. The comparison between the improved model and the original model on the full 24 experimental conditions is provided in the Supporting Information. The results demonstrate the improved prediction

DOI: 10.1021/acs.langmuir.8b04320
Langmuir 2019, 35, 7322−7331

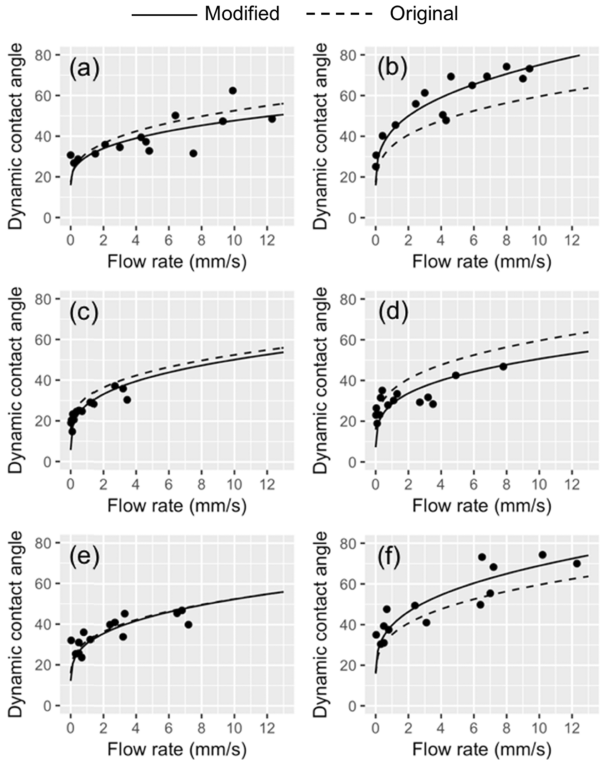

Figure 6. Fitting of Fluorinert/water dynamic contact angle with the water film for (a) Fluorinert/water on the untreated surface; (b) Fluorinert/NaCl solution on the untreated surface; (c) Fluorinert/water on the roughened surface; (d) Fluorinert/NaCl solution on the roughened surface; (e) Fluorinert/water on the wettability modified surface; (f) Fluorinert/NaCl solution on the wettability modified surface. The dashed line and solid line represent the best fit using the original Joos equation and the newly proposed eq 9, respectively.

compared with the original model on the Fluorinert/water fluid pair with the water film.

Forced Imbibition Experiments. To further explore the influence of surface textures relative to other parameters, a second set of experiments was carried out under forced imbibition conditions for two fixed flow rates. These experiments enabled us to test the second hypothesis of this study, that these nanotextures would have a stronger impact on flow than chemical wettability under certain conditions. The interaction between the fluid interface and the solid surface becomes more pronounced in capillary-dominated flow regimes, as suggested by previous experimental studies.[39,58] Studying these dynamics at lower capillary numbers could reveal the flow dynamics and test the applicability of the findings for both viscous flow and capillary dominant flow. Also, the integrated high-velocity microscope imaging system allows the geometry of the two-phase interface to be closely monitored along with its velocity over time. The use of the confocal microscope also enabled image processing that could lead to a mechanistic understanding of these processes. In forced imbibition experiments, the normalized standard deviation of the interface velocity $\left(\frac{dl}{dt}\right)$ is used as a measure of stick/slip behavior along the interface. It is quantified as the standard deviation of the horizontal velocity of the moving interface through a capillary divided by the average velocity value. Table 3 is obtained from the ANOVA results (the complete ANOVA is provided in the Supporting Information) using normalized velocity standard deviation as the response, the roughened surface and wettability modified surface are both compared to the untreated surface.

The results reported in Table 3 suggest that the surface feature contributes to the response variability for both cases, with much larger effects observed for the roughened case. The total percent contribution for the surface feature and its interaction with other factors account for over 50% for the roughened case and only 20% for the wettability-modified case. For the roughened case, the flow rate, surface properties, and the surface, water film interaction has large effects that together account for over 60% of the variability in the velocity standard deviation. For the wettability modified case, effects are more uniform across the four factors, with the water film being the second strongest model term. Surface treatment (untreated, roughened, or wettability modified) shows a significant contribution to the response variation as well as flow rate. The water film is a large contributor for untreated and wettability modified samples but not for roughened samples.

From the analysis of variance (ANOVA), results presented in Table 3, the interplay between surface treatment (wettability modified, roughened) and water film accounts for a significant variance of the response variable. The detailed normalized velocity standard deviation data over the three surfaces with and without water film are shown in the box and whisker plots in

Table 3. Analysis of Variance for the Velocity Standard Deviation (i.e., the Instantaneous Acceleration of the Fluid Contact Line) Collected Using Forced Imbibition Experiments[a]

	roughened			wettability modified		
independent variables and interactions	effect	SoS	% cont.	effect	SoS	% cont.
flow rate	−0.31	0.75	19.82	−0.77	4.79	38.69
water film	−0.05	0.02	0.46	0.52	2.2	17.78
surface	0.34	0.91	24.15	−0.36	1.05	8.47
aqueous chemistry	0.18	0.27	7.13	0.31	0.77	6.21
flow rate + water film	0.01	0	0.03	−0.23	0.42	3.42
flow rate + surface	−0.19	0.28	7.51	0.28	0.63	5.05
water film + surface	0.28	0.65	17.16	−0.29	0.66	5.31
flow rate + aqueous chemistry	0.04	0.02	0.41	0.03	0.01	0.08
water film + aqueous chemistry	−0.03	0.01	0.17	0.28	0.62	4.99
surface + aqueous chemistry	0.01	0	0.027	−0.12	0.11	0.86

[a]Effect coefficient, sum of squares (SoS), and percentage contribution (% cont.) are calculated for both roughened and wettability modified conditions compared with the untreated condition.

DOI: 10.1021/acs.langmuir.8b04320
Langmuir 2019, 35, 7322−7331

Figure 7. Normalized velocity standard deviation values across the three surfaces are very similar when a water film is absent

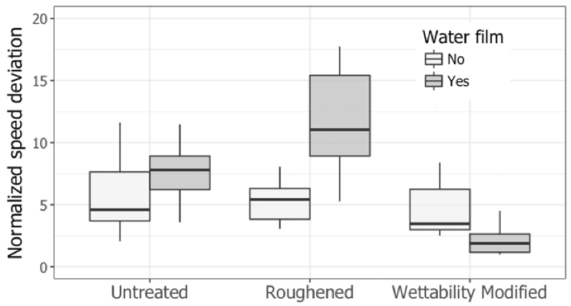

Figure 7. Normalized velocity standard deviation for different surfaces and water films.

but vary significantly when the water film is present. This suggests that the Wenzel regimes qualitatively capture the behavior of our system, i.e., that the presence of a water film dramatically enlarges the differences of the displacement pattern between surfaces.[19]

Water Film Analysis. To understand the interaction of surface feature and water film, we imaged the water film on different surfaces using a confocal microscope. The results, shown in Figure 8, reveal that the untreated surface generally has a thin (10 ± 3 μm thick) and isolated water residual after drainage; the wettability modified surface has a more uniform water film due to enhanced wetting (20 ± 3 μm thick); and roughened surface has an intermediate thickness, but broken water film (varying between 20 and 30 μm in thickness). The water film thickness observed in this work is consistent with what has been previously reported in the literature.[59] The smoothest flow was observed for wettability modified surfaces with a pre-existing wetting film, which is consistent with the literature suggesting that the presence of a wetting film enhances a stable displacement. This velocity standard deviation can be explained by the thickness and the geometry of the water film. Figure 8b indicates that the low-velocity standard deviation, in the case of the wettability modified surface, is linked to the uniformity of the water film. In addition to that, the lower average velocity standard deviation, recorded by the tracking algorithm can be explained by the thickness of the water film.

In the case of the rough capillary, Figure 8c indicates the presence of a water film that may be masking the roughness in some places. However, the velocity standard deviation is the highest when the roughness is combined with the presence of the water film. Qualitative observations of the experimental videos reveal vibrations at the interface, suggesting that repeated instances of fluid pinning were taking place as the fluids moved through the capillary. This pinning can only be linked to the areas of the water film where the thickness varies significantly.

CONCLUSIONS

Glass capillary micromodel experiments were carried out to explore the role that nanoscale roughness on the glass surface plays in multiphase fluid flow. Analysis of variance was used to analyze the relative contribution from the different independent variables based on a modified 2^k factorial design. Surface roughness, wettability, solution chemistry, and the presence of a water film were tested to understand their impact on interface dynamics. Dynamic contact angles were measured as well as the interface velocity standard deviation, which could create instabilities that influence macroscale flow dynamics in porous media through pore-scale processes such as snap-off and Haines jump.

The results indicate that surface roughness, wettability, and the presence of a water film are the most important factors in controlling dynamic contact angle effects. Surface treatment and aqueous chemistry have a statistically significant impact on the dynamic contact angle. The nonaqueous fluid type does impact the results, but it does not interact with any other variables, suggesting these results are generalizable for other fluid plans. Water film does not have a strong impact as a single variable, but its interaction effect with aqueous chemistry and surface feature is statistically significant. These results are used to propose a new empirical equation for predicting dynamic contact angle, using a modified empirical framework based on the Joos equation that also incorporates elements of Wenzel's law to account for surface roughness. This new equation significantly improves the prediction accuracy of experiment data, by taking water film and aqueous chemistry into account. The RMSE of predicting experimental data is reduced up to 67%.

These results advance our mechanistic understanding of the relative importance of the factors controlling contact angle dynamics. Based on the factors that are identified in ANOVA, one-way and two-way effects are important for fully characterizing the behavior of the system. Although the experiments reported here were designed to explore these relationships between system characteristics and multiphase flow, the results suggest that certain aspects of the system, such as different nanostructure morphologies or ionic strength profiles in the aqueous phase, could be explored in greater depth to provide predictive capabilities over a wider range of natural conditions. These results highlight the importance of incorporating a more comprehensive set of factors in pore-scale modeling when predicting macroscopic multiphase flow behaviors.

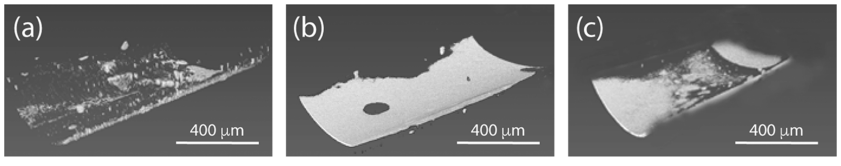

Figure 8. Three-dimensional reconstruction of wetting phase film, under the nonwetting phase, after imbibition under no-flow conditions. (a) Untreated surface; (b) wettability modified surface; and (c) roughened surface.

DOI: 10.1021/acs.langmuir.8b04320
Langmuir 2019, 35, 7322−7331

■ ASSOCIATED CONTENT

Supporting Information

The Supporting Information is available free of charge on the ACS Publications website at DOI: 10.1021/acs.langmuir.8b04320.

Full analysis of variance (ANOVA) results in tabular form (p S2), complete plots of dynamic contact angle results (p S17), and surface profile analysis (p S6) (PDF)

■ AUTHOR INFORMATION

Corresponding Author

*E-mail: andres@virginia.edu.

ORCID

W. B. Bartels: 0000-0003-0890-9350

A. Clarens: 0000-0002-0606-9717

Notes

The authors declare no competing financial interest.

■ ACKNOWLEDGMENTS

This research has been carried out as a part of the SCIPORE Project, ERC-2013-ADG (341225), and via the U.S. National Science Foundation via Awards CBET-1254839 and CBET-1134397. The authors would like to thank Tilly Bouten (Utrecht University) for the technical assistance and access to SEM, and Jason Kerrigan (UVa) for loaning us the high speed camera.

■ REFERENCES

(1) Pinder, G. F.; Gray, W. G. *Essentials of Multiphase Flow and Transport in Porous Media*; Wiley, 2008.

(2) Deng, H.; Fitts, J. P.; Crandall, D.; McIntyre, D.; Peters, C. A. Alterations of Fractures in Carbonate Rocks by CO2-Acidified Brines. *Environ. Sci. Technol.* **2015**, *49*, 10226−10234.

(3) Wang, Y.; Zhang, C.; Wei, N.; Oostrom, M.; Wietsma, T. W.; Li, X.; Bonneville, A. Experimental Study of Crossover from Capillary to Viscous Fingering for Supercritical CO2-Water Displacement in a Homogeneous Pore Network. *Environ. Sci. Technol.* **2013**, *47*, 212−218.

(4) Jamaloei, B. Y.; Kharrat, R.; Asghari, K.; Torabi, F. The Influence of Pore Wettability on the Microstructure of Residual Oil in Surfactant-Enhanced Water Flooding in Heavy Oil Reservoirs: Implications for Pore-Scale Flow Characterization. *J. Pet. Sci. Eng.* **2011**, *77*, 121−134.

(5) Jamaloei, B. Y.; Kharrat, R. Fundamental Study of Pore Morphology Effect in Low Tension Polymer Flooding or Polymer-Assisted Dilute Surfactant Flooding. *Transp. Porous Media* **2009**, *76*, 199−218.

(6) Oughanem, R.; Youssef, S.; Bauer, D.; Peysson, Y.; Maire, E.; Vizika, O. A Multi-Scale Investigation of Pore Structure Impact on the Mobilization of Trapped Oil by Surfactant Injection. *Transp. Porous Media* **2015**, *109*, 673−692.

(7) Schnaar, G.; Brusseau, M. L. Characterizing Pore-Scale Configuration of Organic Immiscible Liquid in Multiphase Systems With Synchrotron X-Ray Microtomography. *Vadose Zone J.* **2006**, *5*, 641.

(8) Geistlinger, H.; Ataei-dadavi, I. Influence of the Heterogeneous Wettability on Capillary Trapping in Glass-Beads Monolayers: Comparison between Experiments and the Invasion Percolation Theory. *J. Colloid Interface Sci.* **2015**, *459*, 230−240.

(9) Iglauer, S.; Al-yaseri, A. Z.; Rezaee, R.; Lebedev, M. CO2 Wettability of Caprocks: Implications for Structural Storage Capacity and Containment Security. *Geophys. Res. Lett.* **2015**, *42*, 9279−9284.

(10) Anderson, W. G. Wettabiility Literature Survery Part 4- Effects of Wettability on Capillary Pressure. *J. Pet. Technol.* **1987**, 1283−1300.

(11) Botto, J.; Fuchs, S. J.; Fouke, B. W.; Clarens, A. F.; Freiburg, J. T.; Berger, P. M.; Werth, C. J. Effects of Mineral Surface Properties on Supercritical CO2 Wettability in a Siliciclastic Reservoir. *Energy Fuels* **2017**, *31*, 5275−5285.

(12) Wang, S.; Tao, Z.; Persily, S. M.; Clarens, A. F. CO2 Adhesion on Hydrated Mineral Surfaces. *Environ. Sci. Technol.* **2013**, 11858−11865.

(13) Al-yaseri, A. Z.; Roshan, H.; Lebedev, M.; Barifcani, A.; Iglauer, S. Dependence of Quartz Wettability on Fluid Density. *Geophys. Res. Lett.* **2016**, 3771−3776.

(14) Al-Menhali, A.; Niu, B.; Krevor, S. Capillarity and Wetting of Carbon Dioxide and Brine during Drainage in Berea Sandstone at Reservoir Conditions. *Water Resour. Res.* **2015**, *51*, 7895−7914.

(15) Raeesi, B.; Morrow, N. R.; Mason, G. Effect of Surface Roughness on Wettability and Displacement Curvature in Tubes of Uniform Cross-Section. *Colloids Surf., A* **2013**, *436*, 392−401.

(16) Li, X.; Fan, X.; Askounis, A.; Wu, K.; Sefiane, K.; Koutsos, V. An Experimental Study on Dynamic Pore Wettability. *Chem. Eng. Sci.* **2013**, *104*, 988−997.

(17) Cassie, A. B. D.; Baxter, S. Large Contact Angles of Plant and Animal Surfaces. *Nature* **1945**, *155*, 21.

(18) Wenzel, R. N. Resistance of Solid Surfaces to Wetting by Water. *Ind. Eng. Chem.* **1936**, *28*, 988−994.

(19) Quéré, D. Wetting and Roughness. *Annu. Rev. Mater. Res.* **2008**, *38*, 71−99.

(20) Zhou, D.; Fayers, F. J.; Orr, F. M. Scaling of Multiphase Flow in Simple Heterogeneous Porous Media. *SPE Reservoir Eng.* **1994**, 173−178.

(21) Kibbey, T. C. G. The Configuration of Water on Rough Natural Surfaces: Implications for Understanding Air-Water Interfacial Area, Film Thickness, and Imaging Resolution. *Water Resour. Res.* **2013**, *49*, 4765−4774.

(22) Tokunaga, T. K. DLVO-Based Estimates of Adsorbed Water Film Thicknesses in Geologic CO 2 Reservoirs. *Langmuir* **2012**, 8001−8009.

(23) Kim, Y.; Wan, J.; Kneafsey, T. J.; Tokunaga, T. K. Dewetting of Silica Surfaces upon Reactions with Supercritical CO2 and Brine: Pore-Scale Studies in Micromodels. *Environ. Sci. Technol.* **2012**, *46*, 4228−4235.

(24) Kim, T. W.; Tokunaga, T. K.; Bargar, J. R.; Latimer, M. J.; Webb, S. M. Brine Film Thicknesses on Mica Surfaces under Geologic CO 2 Sequestration Conditions and Controlled Capillary Pressures. *Water Resour. Res.* **2013**, *49*, 5071−5076.

(25) Geistlinger, H.; Ataei-dadavi, I.; Vogel, H.-J. Impact of Surface Roughness on Capillary Trapping Using 2D-Micromodel Visualization Experiments. *Transp. Porous Media* **2016**, *112*, 207−227.

(26) Girardo, S.; Palpacelli, S.; De Maio, A.; Cingolani, R.; Succi, S.; Pisignano, D. Interplay between Shape and Roughness in Early-Stage Microcapillary Imbibition. *Langmuir* **2012**, *28*, 2596−2603.

(27) Kunz, P.; Zarikos, I. M.; Karadimitriou, N. K.; Huber, M.; Nieken, U.; Hassanizadeh, S. M. Study of Multi-Phase Flow in Porous Media: Comparison of SPH Simulations with Micro-Model Experiments. *Transp. Porous Media* **2015**, 581−600.

(28) Kunz, P.; Nieken, U.; Hassanizadeh, S. M. Study of Wetting Behavior from Low to High Capillary Numbers: A New Model for Liquid-Solid Interactions on the Pore-Scale.

(29) Singh, K.; Menke, H.; Andrew, M.; Lin, Q.; Rau, C.; Blunt, M. J.; Bijeljic, B. Dynamics of Snap-off and Pore-Filling Events during Two-Phase Fluid Flow in Permeable Media. *Sci. Rep.* **2017**, *7*, No. 5192.

(30) Armstrong, R. T.; McClure, J. E.; Berrill, M. A.; Rücker, M.; Schlüter, S.; Berg, S. Beyond Darcy's Law: The Role of Phase Topology and Ganglion Dynamics for Two-Fluid Flow. *Phys. Rev. E* **2016**, No. 043113.

(31) Karadimitriou, N. K.; Joekar-Niasar, V.; Hassanizadeh, S. M.; Kleingeld, P. J.; Pyrak-Nolte, L. J. A Novel Deep Reactive Ion Etched (DRIE) Glass Micro-Model for Two-Phase Flow Experiments. *Lab Chip* **2012**, *12*, 3413−3418.

DOI: 10.1021/acs.langmuir.8b04320
Langmuir 2019, 35, 7322−7331

(32) Mirchi, V.; Saraji, S.; Goual, L.; Piri, M. Dynamic Interfacial Tension and Wettability of Shale in the Presence of Surfactants at Reservoir Conditions. *Fuel* **2015**, *148*, 127−138.
(33) Farokhpoor, R.; Bjørkvik, B. J. A.; Lindeberg, E.; Torsæter, O. Wettability Behaviour of CO2 at Storage Conditions. *Int. J. Greenhouse Gas Control* **2013**, *12*, 18−25.
(34) Girardo, S.; Palpacelli, S.; De Maio, A.; Cingolani, R.; Succi, S.; Pisignano, D. Interplay between Shape and Roughness in Early-Stage Microcapillary Imbibition. *Langmuir* **2012**, *28*, 2596−2603.
(35) Washburn, E. W. The Dynamics of Capillary Flow. *Phys. Rev.* **1921**, *17*, 273−283.
(36) Sheng, P.; Zhou, M. Immiscible-Fluid Displacement: Contact-Line Dynamics and the Velocity-Dependent Capillary Pressure. *Phys. Rev. A* **1992**, *45*, 5694−5708.
(37) Popescu, M. N.; Ralston, J.; Sedev, R. Capillary Rise with Velocity-Dependent Dynamic Contact Angle. *Langmuir* **2008**, *24*, 12710−12716.
(38) Brochard-Wyart, F.; De Gennes, P. G. Dynamics of Partial Wetting. *Adv. Colloid Interface Sci.* **1992**, *39*, 1−11.
(39) Blake, T. D. The Physics of Moving Wetting Lines. *J. Colloid Interface Sci.* **2006**, *299*, 1−13.
(40) Bracke, M.; Voeght, F.; Joos, P. The Kinetics of Wetting: The Dynamic Contact Angle. *Prog. Colloid Polym. Sci.* **1989**, *149*, 142−149.
(41) Joos, P.; Remoortere, V. A. N.; Bracke, M. The Kinetics of Wetting in a Capillary. *J. Colloid Interface Sci.* **1990**, *136*, 189−197.
(42) Cox, R. G. The Dynamics of the Spreading of Liquids on a Solid Surface. Part 1. Viscous Flow. *J. Fluid Mech.* **1986**, *168*, 169−194.
(43) Andrew, M.; Bijeljic, B.; Blunt, M. J. Pore-by-Pore Capillary Pressure Measurements Using X-Ray Microtomography at Reservoir Conditions: Curvature, Snap-Off, and Remobilization of Residual CO 2. *Water Resour. Res.* **2014**, *50*, 8760−8774.
(44) Chaudhary, K.; Bayani Cardenas, M.; Wolfe, W. W.; Maisano, J.; Ketcham, R.; Bennett, P. C. Pore-Scale Trapping of Supercritical CO 2 and the Role of Grain Wettability and Shape. *Geophys. Res. Lett.* **2013**, *40*, 3878−3882.
(45) Zhao, B.; MacMinn, C. W.; Juanes, R. Wettability Control on Multiphase Flow in Patterned Microfluidics. *Proc. Natl. Acad. Sci. U.S.A.* **2016**, *113*, 10251−10256.
(46) Mazurczyk, R.; El Khoury, G.; Dugas, V.; Hannes, B.; Laurenceau, E.; Cabrera, M.; Krawczyk, S.; Souteyrand, E.; Cloarec, J. P.; Chevolot, Y. Low-Cost, Fast Prototyping Method of Fabrication of the Microreactor Devices in Soda-Lime Glass. *Sens. Actuators, B* **2008**, *128*, 552−559.
(47) Xiong, J.; Das, S. N.; Kar, J. P.; Choi, J.-H.; Myoung, J.-M. A Multifunctional Nanoporous Layer Created on Glass through a Simple Alkali Corrosion Process. *J. Mater. Chem.* **2010**, *20*, 10246.
(48) Yao, L.; He, J. Recent Progress in Antireflection and Self-Cleaning Technology - From Surface Engineering to Functional Surfaces. *Prog. Mater. Sci.* **2014**, *61*, 94−143.
(49) Du, X.; He, J. Structurally Colored Surfaces with Antireflective, Self-Cleaning, and Antifogging Properties. *J. Colloid Interface Sci.* **2012**, *381*, 189−197.
(50) Stalder, A. F.; Kulik, G.; Sage, D.; Barbieri, L.; Hoffmann, P. A Snake-Based Approach to Accurate Determination of Both Contact Points and Contact Angles. *Colloids Surf., A* **2006**, *286*, 92−103.
(51) Aggelopoulos, C. A.; Robin, M.; Perfetti, E.; Vizika, O. CO2/CaCl2 Solution Interfacial Tensions under CO2 Geological Storage Conditions: Influence of Cation Valence on Interfacial Tension. *Adv. Water Resour.* **2010**, *33*, 691−697.
(52) Kang, K. H. How Electrostatic Fields Change Contact Angle in Electrowetting. *Langmuir* **2002**, *18*, 10318−10322.
(53) Jones, R.; Pollock, H. M.; Cleaver, J. A. S.; Hodges, C. S. Adhesion Forces between Glass and Silicon Surfaces in Air Studied by AFM: Effects of Relative Humidity, Particle Size, Roughness, and Surface Treatment. *Langmuir* **2002**, *18*, 8045−8055.
(54) Steitz, R.; Jaeger, W.; Klitzing, R. Influence of Charge Density and Ionic Strength on the Multilayer Formation of Strong Polyelectrolytes. *Langmuir* **2001**, *17*, 4471−4474.
(55) Kuchin, I. V.; Matar, O. K.; Craster, R. V.; Starov, V. M. Influence of the Disjoining Pressure on the Equilibrium Interfacial Profile in Transition Zone Between a Thin Film and a Capillary Meniscus. *Colloids Interface Sci. Commun.* **2014**, *1*, 18−22.
(56) Mahani, H.; Berg, S.; Rijswijk, T. H.; Bartels, W. Kinetics of Low-Salinity-Flooding Effect. *SPE J.* **2015**, 8−20.
(57) Kinniburgh, D. G. General Purpose Adsorption Isotherms. *Environ. Sci. Technol.* **1986**, *20*, 895−904.
(58) Blake, T. D.; Shikhmurzaev, Y. D. Dynamic Wetting by Liquids of Different Viscosity. *J. Colloid Interface Sci.* **2002**, *253*, 196−202.
(59) Cachile, M.; Chertcoff, R.; Calvo, A.; Rosen, M.; Hulin, J. P.; Cazabat, A. M. Residual Film Dynamics in Glass Capillaries. *J. Colloid Interface Sci.* **1996**, *182*, 483−491.

DOI: 10.1021/acs.langmuir.8b04320
Langmuir 2019, 35, 7322−7331